Tellus (1990), *42A*, 482–495

Dynamic coupling of sea ice and water for an ice field with free boundaries

By MATTI LEPPÄRANTA, *Finnish Institute of Marine Research, P.O. Box 33, SF-00931 Helsinki, Finland* and ANDERS OMSTEDT, *Swedish Meteorological and Hydrological Institute, S-601 76 Norrköping, Sweden*

(Manuscript received 27 July 1988; in final form 4 July 1989)

ABSTRACT

Ice–ocean dynamics is investigated using field data and a transient ice–ocean model. The measurements were made in April 1975 in the Bothnian Bay in an ice patch (100 km across) with free boundaries. The data consist of velocity time series of wind, ice, and currents at depths of 7, 10, 20 and 30 m from the ice. The ice–ocean model is used to examine the characteristics of the observations; the model consists of an unsteady free ice drift model and a transient Ekman flow model, which uses a two-equation turbulence model to achieve closure. For the surface wind at the altitude of 10 m, the estimated wind factor was 1.9%, and the deviation angle 21°, the ice-wind correlation being 0.90. The wind factor value is slightly low, probably due to biased wind data. The optimized oceanic boundary layer parameters are: roughness length 0.05 m and displacement height (due to ice ridge keels) 5 m. The model simulations predict significant inertial oscillations in the whole ice–ocean system, but in the ice measurements, they are missing and appear as highly damped in the current measurements. The reason for this discrepancy is probably due to the internal friction of the ice. Using the ocean model forced by observed ice drift data, a better fit to the current data was achieved and the inertial oscillations in the current calculations were correctly damped.

1. Introduction

The coupling between ice drift and underlying currents has been one of the basic problems in sea ice dynamics. The traditional solution is to let the sea have a given background current and exert a passive drag force to the ice. This force is non-zero as soon as the ice velocity differs from the background current, and the adjustment of the frictional boundary layer is taken to be immediate. Thus, the traditional solution does not allow the ice to influence the ocean current system and, on the other hand, in oceanographic modelling of ice-covered seas, the ice has generally been taken as a passive transmitter of the wind energy to the oceanic boundary layer.

In the present decade, the need to develop advanced ice–ocean models has greatly increased. In particular, this has been true in the Marginal Ice Zone (MIZ) investigations (Wadhams et al., 1981; MIZEX Group, 1986). In the MIZ, the dynamic coupling of the two media is of key importance, and consequently, several kinds of coupled models have been developed (e.g., Røed and O'Brien, 1983; Overland et al., 1984; Ikeda, 1985 and 1986; Mellor et al., 1986; Lemke, 1987; Svensson and Omstedt, 1989). These coupled models, however, have so far lacked a full description of the internal friction of the ice, and this has been considered reasonable, owing to the relatively loose appearance of the MIZ ice and the presence of a free boundary.

The ice does have a strongly active role in the air–ice–ocean dynamics. External forcing variations become highly damped in the ice due to the internal friction, and this also means that the ice causes a significant modification to the air-sea momentum transfer. Modelling results and field data show the damping phenomenon clearly in the MIZ (Leppäranta and Hibler, 1985, 1987).

In general, when the ice–ocean dynamic coupling is investigated, special attention must be paid to the way the ice behaves. Although the ice provides an excellent platform for oceanic boundary layer studies, it is not a passive tracer of the current system. This paper provides an illustration of the active role of the ice in the high frequency regime in ice–ocean dynamics.

In the present work, the dynamic coupling of ice and water is studied using field data and a mathematical model. The observations were made in the Bothnian Bay, Baltic Sea, in April 1975, when the drift of an ice patch (100 km across) with free boundaries was measured together with the currents beneath the ice and wind. The situation is a very good apparent free ice drift (no internal friction) case.

The model calculations are based upon a transient ice–ocean model. For the ice, the free drift momentum equation is used. The mathematical formulation for the ocean is the conservation equations for momentum and salinity in their one-dimensional form. The turbulent exchange coefficients are calculated using a two-equation model of turbulence (the so-called k–ε model). Based on the model simulations, optimized oceanic boundary layer parameters are presented. The best fit of the ice–ocean model to the ice drift data gives a correlation of 0.87, but the result is not better than that of a simple purely wind-driven ice model.

2. Field measurements

2.1. Data

The present data are from a Finnish ice dynamics experiment, which was performed in April 1975 in the Bothnian Bay, Baltic Sea (Fig. 1). The basic results of this experiment have been presented in Leppäranta (1989). The base was R/V Aranda, moored to an ice floe (Fig. 2). The measurement programme lasted from 7 April, 21 hrs, to 17 April, 9 hrs (Finnish time = GMT + 2 hrs), but complete time series are only available through 10–17 April. The initial location of R/V Aranda was 65°01′ North 23°32′ East, and its net displacement was 27 km south during the experiment.

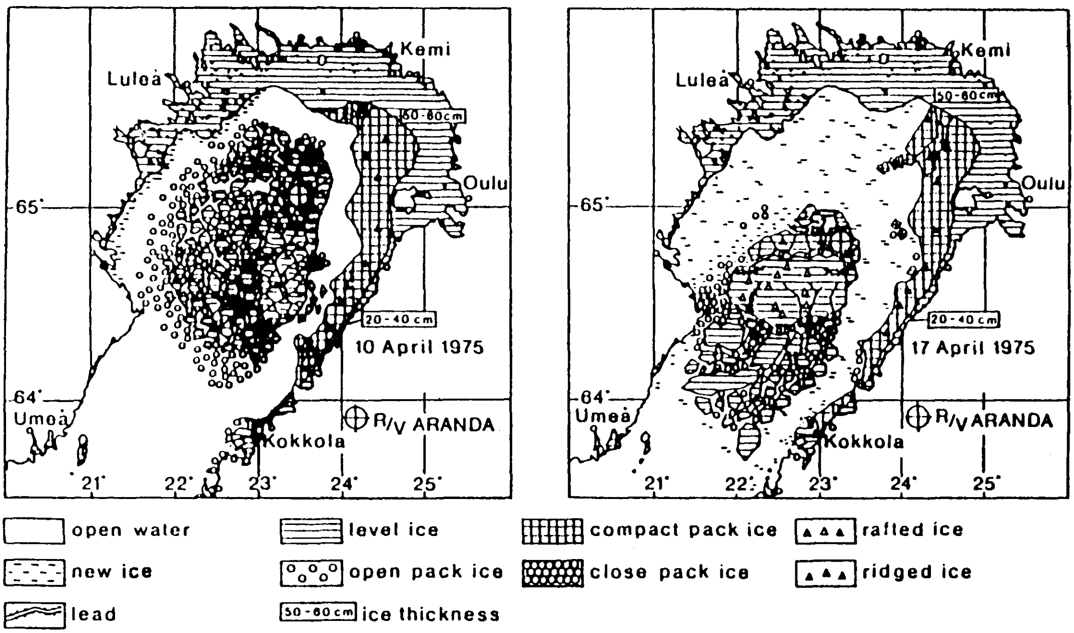

Fig. 1. The ice situation in the Bothnian Bay in the beginning and at the end of the experiment.

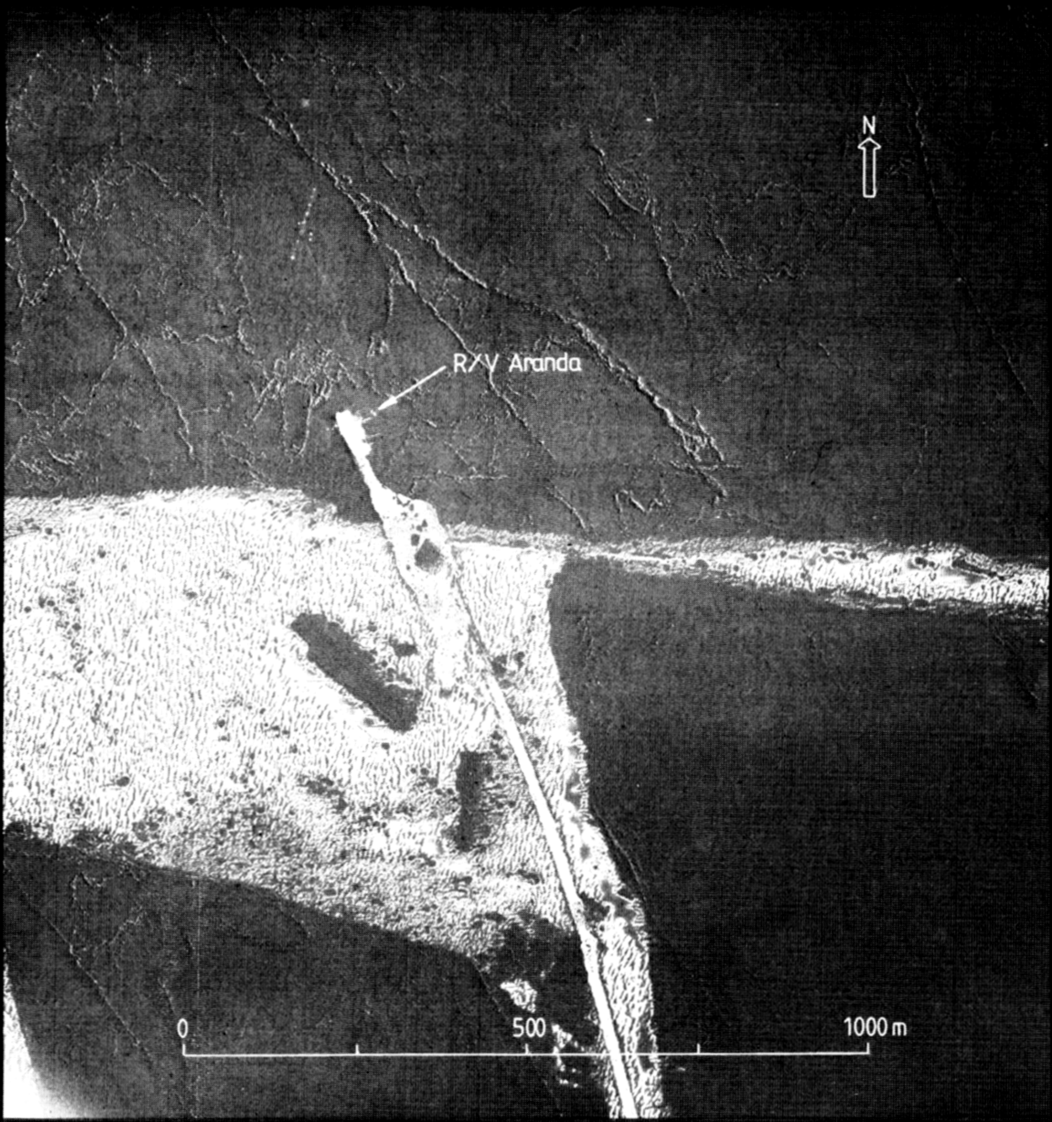

Fig. 2. Aerial photograph of the base, 14 April, 1975, 13 hrs. The location of the current recorders was some 30–50 m to the right from the ship.

The ice season 1974/75 was very mild in the Baltic Sea. In April the ice coverage of the Bothnian Bay was only some 60% (Fig. 1). At the coast and in the skerries, there was a level fast ice area, and a narrow immobile ridged zone occurred at the fast ice boundary in the eastern side of the basin. This zone was kept immobile basically by grounded ridges. The drifting pack ice was concentrated in a patch (around 100 km across) which was not in contact with the immobile ice. The compactness of the patch increased from 70 to almost 100% due to ice convergence during the period of the experiment. According to aerial photography on 14 April 1975, 13 hrs, when the ice pack had closed up, the compactness was 0.96. The average level ice thickness was about 0.4 m, and it was estimated that the amount of ridged ice was about half of the level ice mass. Consequently, the average total ice thickness was approximately 0.6 m. There were basically two types of ice present: thick snow-covered ice and thin bare ice. Ice floes in the patch were not frozen together. The number of ice ridges was estimated to 4–8 per one kilometer track.

The measurements used in this paper are the velocity time series of the surface wind, ice, and currents beneath the ice. The wind was measured hourly with R/V Aranda's anemometer and direction vane located above the bridge. The wind speed observations were corrected by dividing by 1.15 to get the best estimates for the surface wind at the altitude of 10 m, as recommended by Kahma and Leppäranta (1981). The anemometer height is 17 m which would mean a reduction factor of 1.07 if the measurements were unbiased; the rest of the 1.15 correction factor is due to the ship's hull effect compressing the stream lines above. However, the correction factor 1.15 refers to the wind blowing from the direction of Aranda's bow, and, as shown in Kahma and Leppäranta (1981), the factor may be as large as 1.40 when the wind blows perpendicularly to the bow direction. The drift of the ice was obtained from hourly Decca coordinates of the ship. The Decca system is rather good for displacement measurements and gives one-hour average velocities at the accuracy of 0.005 m/s.

The currents beneath the ice were measured with Alexejev current recorders made in the Soviet Union. The measurements are quasi-Lagrangian, made from the drifting ice floe where R/V Aranda was moored to. They describe integrated speed and instantaneous direction at 5-min intervals; the threshold speed is 0.04 m/s and the accuracy about 0.03 m/s. The measurement depths were 7, 10, 20 and 30 m, which all lie within the layer of frictional influence of the ice. Ice ridges with deeper keels than 7 m were probably rare (less than 1 km^{-1}). Unfortunately hydrographic data are not available. However, on the basis of our experience during other ice seasons it is most likely that there was a homogeneous upper layer of 20–40 m depth. The depth of the sea was 60–100 m below the moving base.

The raw data were first smoothed by removing frequencies higher than 0.5 cycles per hour (cph), and the smoothed records were then resampled at 1-h intervals. These hourly time series are used in the present analysis.

2.2. Results

The average velocities are shown in Fig. 3. In the average velocities, the ice drift direction deviates 15.9° to the right from the wind direction and the ice speed is 2.0% of the wind speed. Beneath the ice there is a rapid shear in the uppermost 7 m. Between 7 and 10 m the current speed is approximately a constant and rotates about 40° clockwise, and between 10 and 30 m the velocity decreases and rotates. The velocity profile thus shows Ekman-type behaviour.

The ice drift followed the wind with a time-lag of less than one hour, which was the measurement interval. The correlation between these two time series was certainly better than observed in other experiments in this basin (e.g., Leppäranta, 1981). Linear regression analysis of the ice and wind velocities gave the wind factor of 1.9% and

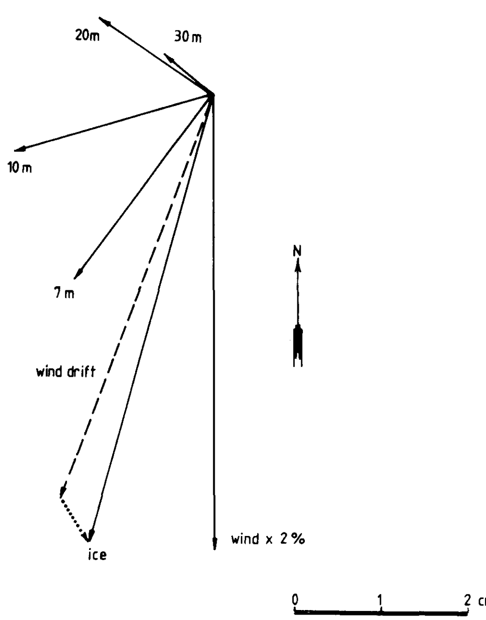

Fig. 3. The average velocities of ice, wind and currents during the experiment through 10 to 17 April. Also shown is the optimized wind-driven ice drift vector (dashed line).

deviation angle of 21° (note: surface wind, altitude 10 m). The correlation coefficient was as high as 0.90. This optimized average wind-driven ice velocity vector is also shown in Fig. 3. The difference between the optimized and observed ice velocities shows the average resultant velocity when the wind effect has been eliminated. Note that this velocity does not coincide with the average currents at 20–30 m depth. The difference vector is, however, small. The wind factor value is rather low, probably owing to biased wind data; in earlier studies the wind factor has been estimated to 2.5–3.0% (e.g., Omstedt, 1980; Leppäranta, 1981).

As described in Leppäranta (1989), the measurements showed that velocity fluctuations were larger in the ice than in the water, but in the water there was not much difference. It seemed that when the speeds were greater than about 0.05 m/s, the ice mainly drove the boundary layer beneath it and not vice versa. Even the deepest current, 30 m depth, seemed to be affected by the ice, and thus the layer of frictional influence of the ice was probably deeper than 30 m.

The spectra of all the velocity time series are shown in Fig. 4. The spectra of ice and 2% wind velocities coincide quite well through all frequencies down to the Nyqvist frequency of 0.5 cycles per hour (cph). Comparing the current spectra with the ice velocity spectrum it can be seen that at low frequencies ice has more variance than currents, but at high frequencies the opposite is true. The division is approximately at the frequency of 0.05 cph (or one cycle per day). Between 0.05 and 0.15 cph the ice velocity spectrum is somewhat above the wind spectrum and follows the form of the mean current spectrum quite well on a lower level. The form of the spectra suggests that the ice has obtained kinetic energy from the sea at near-inertial frequencies. The measurement noise level in the ice velocity spectrum is a little less than 0.5 $cm^2 s^{-2}$/cph. According to the present state of knowledge, ice floe bumping effects to the ice velocity field are very small (Martin and Becker, 1987).

The current spectra (Fig. 4b) show largest fluctuations to occur at 20 m depth, but in general the spectra for the various depths do not differ much from each other. The inertial signal can be observed at all levels and is clearest at 20 and 30 m depths—the inertial period is 13.2 h (0.076 cph) at the location of the experiment.

The coherences between ice, wind and vertically integrated current velocities are shown in

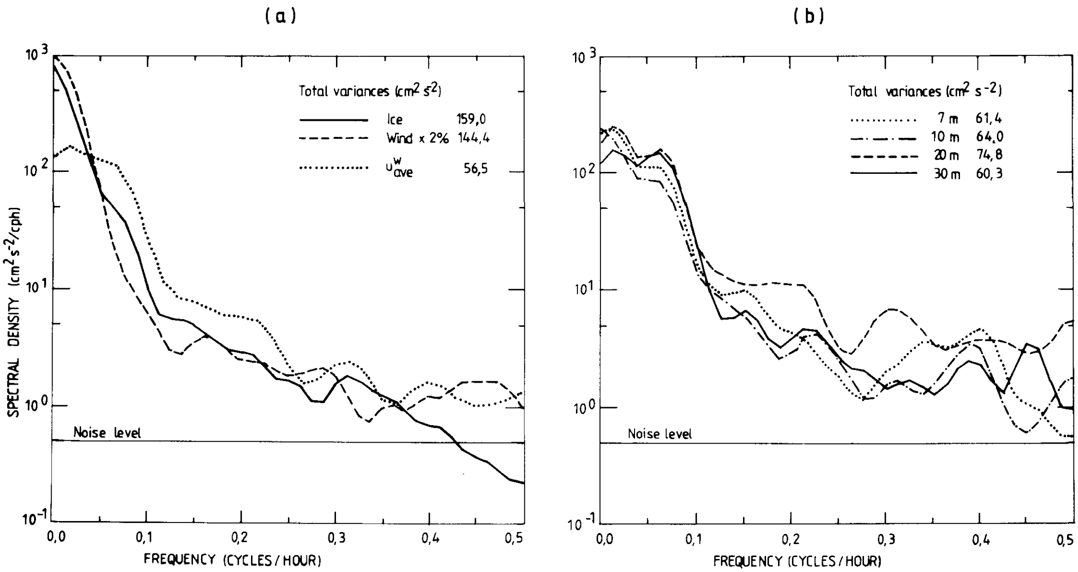

Fig. 4. The velocity spectra: (a) Ice, 2% wind and average current from 7 to 30 m, and (b) currents at the four measurement depths. The 90% confidence interval is 1.1 log units for the velocity components.

Fig. 5. They illustrate clearly the difference in high and low frequency regimes in ice motion—the division at about one half-day or inertial cycle. The low frequencies are dominated by wind, whereas the high frequencies are dominated by the currents. In frequency regimes with significant coherence no significant non-zero phases appeared.

A very high peak appears in the ice–current coherence at about -0.3 cph. The reason for this is unknown, but likely just due to the nature of ice movement: note that the current is actually the relative current measured from ice floe plus floe velocity. The fact that a similar but low peak appears in the ice–wind coherence supports the reality of this phenomenon.

The coherences between ice velocity and currents at various depths were very similar to the ice–current spectra shown in Fig. 5. The significant regime in high frequencies just became narrower with depth. The relative movement between ice and water was significantly coherent only at frequencies lower than 0.1 cph except for a trace of the -0.3 cph peak at the depth of 7 m.

To sum up, the present case fulfills the conditions for what one would think represents an almost ideal free drift case. In the following we shall examine the data through model simulations in order to see if internal friction influences the ice drift.

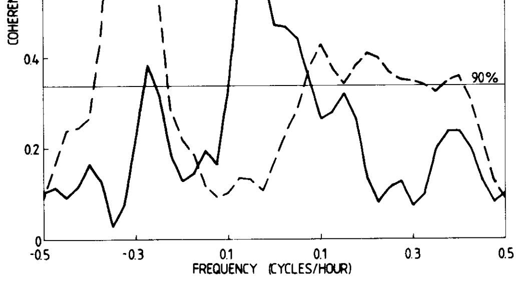

Fig. 5. The coherence between ice and wind (fully drawn line) and between ice and average current (dashed line) from 7 to 30 m depth. The straight solid line shows the 90% significance level.

3. The ice–ocean model

3.1. Introduction

Several models of the free ice drift and the ocean structure beneath the ice are available. As half meter thick ice in general responds quite rapidly to wind changes (within less than one hour), most models start from the steady state approximation. However, even though the ice responds rapidly to the wind, the ocean response is much slower, order of days corresponding to some inertial periods. The oceanic time scale may thus interfere with the time scale of the ice implying that the transient forcing as well as the transient response needs to be considered in the ice–ocean modelling.

A common transient feature in the ice–ocean response is the presence of inertial oscillations; for the Baltic Sea, the report by Gustafson and Kullenberg (1936) during the ice-free season is a standard work. Inertial oscillations in the sea ice drift have also been observed (e.g., Ono, 1978; McPhee, 1978). The observations from the Arctic Ocean (McPhee, 1978) illustrated that the inertial response varies from summer to winter season. During freeze-up periods, the ice becomes rigid and inhibits short period motions. During summer, the ice becomes more loose and mobile, with higher tendency to inertial oscillations. Near inertial current oscillations in the presence of sea ice were also reported from the Bering Sea by Lagerloef and Muench (1987). The presence of sea ice seemed to increase the oscillations during spring time through restratification of the water caused by the melting ice.

3.2. Basic assumptions

The present model is restricted to horizontally homogeneous flows with ice drifting on top of a salinity-stratified ocean. Lateral effects are thus not dealt with. Melting and freezing effects are also neglected. The turbulent mixing is assumed to be caused by current shear and is damped by buoyancy and dissipation. The turbulent mixing is described by exchange coefficients, which together with gradient laws exclude counter gradient fluxes. Two roughness length scales had to be considered at the ice–water interface: ordinary small scale floe bottom roughness and ice ridge keels. These are taken into account using the roughness length and displacement height in the boundary layer equations. This is a standard procedure when modelling wind profiles above a vegetation surface (e.g., Oke, 1981) and is assumed to be appropriate also for the oceanic boundary layer beneath pack ice. Wave drag is not dealt with. The ice drift is modelled with the unsteady free drift equation.

The model employed extends the work by Omstedt et al. (1983) by introducing the ice drift equations and new boundary conditions at the ice–water interface.

3.3. *Mathematical formulation*

Within the assumptions made, the mean ice and ocean equations read:

Ice equations

$$\rho_i \frac{\partial}{\partial t} U_i = \frac{\tau_x^{\mathrm{a}}}{H_i} + \frac{\tau_x^{\mathrm{w}}}{H_i} + f\rho_i V_i, \tag{1}$$

$$\rho_i \frac{\partial}{\partial t} V_i = \frac{\tau_y^{\mathrm{a}}}{H_i} + \frac{\tau_y^{\mathrm{w}}}{H_i} - f\rho_i U_i, \tag{2}$$

where t is the time, U_i and V_i are the east and north ice drift components, H_i is the ice thickness, and ρ_i is the ice density. The wind stress on the upper ice surface and the water stress on the lower ice surface are denoted by τ_x^{a}, τ_y^{a} and τ_x^{w}, τ_y^{w}, respectively, and f is the Coriolis parameter.

Ocean equations:

$$\frac{\partial \rho U}{\partial t} = \frac{\partial}{\partial z}\left(\nu_{\mathrm{T}} \frac{\partial \rho U}{\partial z}\right) + f\rho V, \tag{3}$$

$$\frac{\partial \rho V}{\partial t} = \frac{\partial}{\partial z}\left(\nu_{\mathrm{T}} \frac{\partial \rho V}{\partial z}\right) - f\rho U, \tag{4}$$

$$\frac{\partial S}{\partial t} = \frac{\partial}{\partial z}\left(\frac{\nu_{\mathrm{T}}}{\sigma_{\mathrm{S}}} \frac{\partial S}{\partial z}\right), \tag{5}$$

$$\rho = \rho_0(1 + \beta S), \tag{6}$$

where z is the vertical space coordinate, U and V are the current components, ν_{T} is the kinematic eddy viscosity, S is the salinity, σ_{S} is the Schmidt number, ρ is the density, ρ_0 a reference density, and β a constant.

The forcing of the ice–ocean system is through the wind stress:

$$\tau_x^{\mathrm{a}} = \rho_{\mathrm{a}} C_{\mathrm{d}}^{\mathrm{a}} W^{\mathrm{a}} U^{\mathrm{a}}, \tag{7}$$

$$\tau_y^{\mathrm{a}} = \rho_{\mathrm{a}} C_{\mathrm{d}}^{\mathrm{a}} W^{\mathrm{a}} V^{\mathrm{a}}, \tag{8}$$

where U^{a} and V^{a} are the wind components, W^{a} is the wind speed, ρ_{a} is the air density and $C_{\mathrm{d}}^{\mathrm{a}}$ is the air drag coefficient.

The boundary conditions at the ice–water interface assume that the ice drift is equal to the water velocity at a constant depth, equal to the sum of the displacement (d) and roughness (z_0^{w}) heights. The water stress components in eqs. (1) and (2) are then calculated by the ocean model through $\tau_x^{\mathrm{w}} = \nu_{\mathrm{T}} \partial \rho U/\partial z$, and $\tau_y^{\mathrm{w}} = \nu_{\mathrm{T}} \partial \rho V/\partial z$ at $z = d + z_0^{\mathrm{w}}$. The introduction of the displacement height implies that the ice–water stress is not associated with an inner ice/water region where from drag probably is significant. For the lower ocean boundary, zero velocities are used. The boundary conditions for the salinity are zero-flux conditions.

Turbulence model

The eddy viscosity coefficients are modelled on the basis of a two-equation model of turbulence, one equation for turbulent kinetic energy, k, and one equation for its dissipation rate, ε. This is known as the k–ε model. The generation of turbulence is calculated from shear production associated with the velocity difference between ice and water. Buoyancy effects due to melting and freezing are not considered. The destruction of turbulence is calculated from the dissipation rate and the buoyancy due to a stable salinity-stratified ocean.

The equations read:

$$\frac{\partial k}{\partial t} = \frac{\partial}{\partial z}\left(\frac{\nu_{\mathrm{T}}}{\sigma_{\mathrm{k}}} \frac{\partial k}{\partial z}\right) + P_{\mathrm{s}} + P_{\mathrm{b}} - \varepsilon, \tag{9}$$

$$\frac{\partial \varepsilon}{\partial t} = \frac{\partial}{\partial z}\left(\frac{\nu_{\mathrm{T}}}{\sigma_{\varepsilon}} \frac{\partial \varepsilon}{\partial z}\right) + \frac{\varepsilon}{k}(C_{1\varepsilon} P_{\mathrm{s}} + C_{3\varepsilon} P_{\mathrm{b}} - C_{2\varepsilon}\varepsilon), \tag{10}$$

$$P_{\mathrm{s}} = \nu_{\mathrm{T}}\left[\left(\frac{\partial U}{\partial z}\right)^2 + \left(\frac{\partial V}{\partial z}\right)^2\right], \tag{11}$$

$$P_{\mathrm{b}} = \nu_{\mathrm{T}} g \frac{\beta}{\sigma_{\mathrm{S}}} \frac{\partial S}{\partial z}, \tag{12}$$

$$\nu_{\mathrm{T}} = C_\mu \frac{k^2}{\varepsilon}, \tag{13}$$

where P_s is the production of turbulent kinetic energy due to shear, P_b is destruction due to buoyancy, σ_k and σ_ε are Prandtl/Schmidt numbers, and C_μ, $C_{1\varepsilon}$, $C_{2\varepsilon}$ and $C_{3\varepsilon}$ are constants.

The surface boundary conditions for k and ε are related to the friction velocity. At the lower boundary, a zero flux condition is used. For a general description of the turbulence model, the reader is referred to Svensson (1979) or Rodi (1987). The general equation solver PROBE (Svensson, 1986) has been used in the present calculations. The numerical solution of inertial oscillation was tested and found to be grid- and time-step independent. This was achieved by a grid with 40 cells covering a depth of 80 m and a time step equal to 60 s.

The fixed model constants are given in Table 1. The tuning or calibration constants are air drag coefficient, displacement height and roughness length, to be determined through model simulations.

3.4. *Details of calculations*

Some different types of model runs have been performed. Firstly, the full ice–ocean model was forced with hourly measured winds. Secondly, the ocean model was forced with hourly measured ice velocities. Thirdly, the ice velocity was calculated only on the basis of wind forcing, i.e., the classical purely wind-driven case. To investigate the role of high frequency wind variations, the full model was also run with wind velocity smoothed by removing frequencies higher than one cycle per day. Some further idealized model runs are also given and compared with results from other sea areas.

The stratification effect was modelled by changing the water salinity from 3.5 to 4.1‰ with a mixed layer depth of 40 m, which are typical Bothnian Bay values.

Table 1. *Model constants*

Constant		Value	Unit
C_μ	constant in the turbulence model	0.09	
$C_{1\varepsilon}$	constant in the turbulence model	1.44	
$C_{2\varepsilon}$	constant in the turbulence model	1.92	
$C_{3\varepsilon}$	constant in the turbulence model	0.8	
σ_k	Prandtl/Schmidt number	1.4	
σ_ε	Prandtl/Schmidt number	1.3	
σ_s	Schmidt number	1.0	
β	constant in the equation of state	$8\cdot10^{-4}$	‰$^{-1}$
ρ_0	reference density	10^3	kg m^{-3}
f	Coriolis parameter	$1.3\cdot10^{-4}$	s^{-1}
ρ_a	air density	1.3	kg m^{-3}
ρ_i	ice density	$9.1\cdot10^2$	kg m^{-3}
H_i	ice thickness	0.6	m

4. Model calculations versus observations

4.1. *General*

In Fig. 6, the ice and wind velocity time series for the period of the experiment are illustrated. The wind was mostly weak or moderate; on 11–12 April a period of strong northerly winds occurred and, additionally, southwesterly winds of around 10 m/s occurred on 13 April. The motion of the ice field followed the wind remarkably well. The ice–wind velocity correlation was as high as 0.90. As was discussed in Subsection 2.2, the wind factor was low (1.9%), probably owing to the biased wind data. The only clear single occurrence of deviation from the free wind drift case occurred on 11 April. The variance not explained by the wind must be caused by the currents or the internal friction within the ice field.

The present full ice–ocean model contains three basic calibration factors: the wind drag coefficient, the displacement height (depth) due to ice ridge keels, and the roughness length at the ice–water interface. The drag coefficient and the roughness length were calibrated by comparing measured and calculated ice drift velocities. The value obtained for the drag coefficient is in good agreement with known field measurements (Joffre, 1984). The displacement height, necessary to introduce owing to ice ridge keels, was estimated to 5 m by comparing measured and calculated currents. The calibrated values are shown in Table 2. These parameters (roughness

Table 2. *Calibration constants of the model*

Constant		Value	Unit
C_d^a	air drag coefficient	$1.8\cdot10^{-3}$	
z_0^w	ice–water roughness length	0.05	m
d	displacement height	5	m

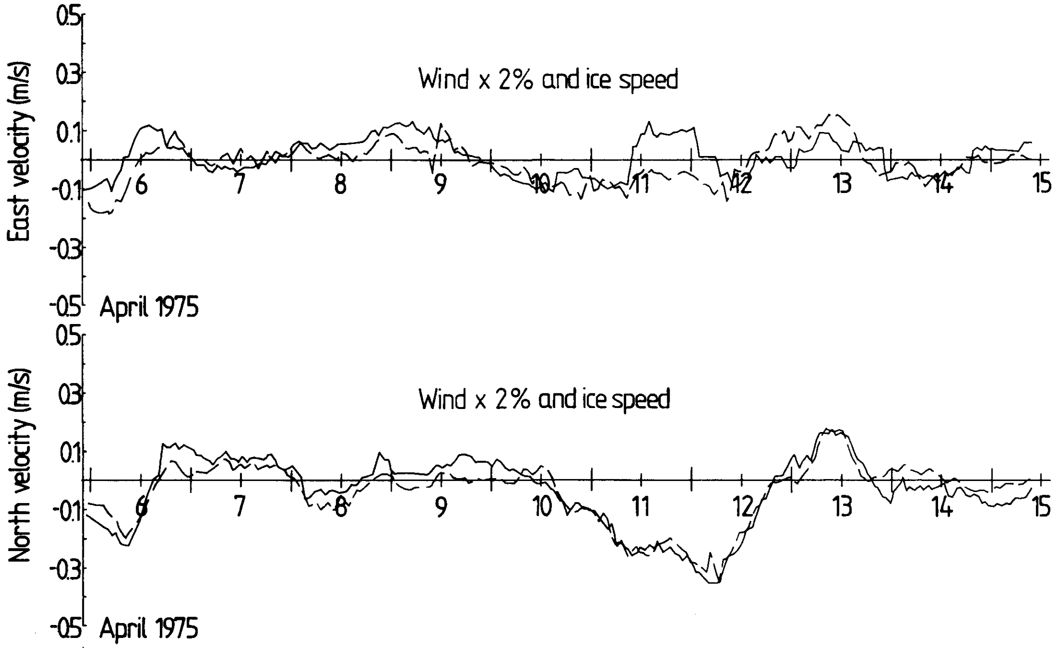

Fig. 6. Measured wind (solid lines) and ice velocities (broken lines).

length 0.05 m, displacement height 5 m) are the first estimated values based on joint ice and sea velocity observations in the Baltic Sea.

4.2. *Ice–ocean model*

In Fig. 7, the results from the full ice–ocean model are given together with the measurements. The main discrepancy between the measured and calculated ice velocities are due to inertial oscillations, present in the calculations but not in the measurements.

This discrepancy in the ice movement seems to appear also in the current velocities, apparently due to the ice motion acting as a boundary condition to the ocean dynamics damping the high frequency fluctuations. The prediction of inertial oscillations in a transient boundary layer model is not surprising. In the atmospheric boundary layer models too much inertial energy is in general predicted (e.g., Egger and Schmid, 1988).

In the ocean, however, inertial oscillations are a common feature, and the question in the present simulation is which processes are the most likely to explain the damping. The main reason is probably the internal friction in the drifting ice. With no inertial oscillations in the ice, inertial oscillations must stay weak in the ocean, too. However, lateral effects in the ocean may also play a significant role.

The correlation between the measured and calculated ice velocity was 0.87. This is slightly less than the direct ice–wind correlation (0.90) which is likely due to the inertial oscillation problem. The most notable single deviation occurred on 11 April. The difference was largest at the depth of 20 m.

The coherence between the observed and calculated ice velocities was very similar to the pure ice–wind coherence in observations. That is, there is no particular frequency band, where the model would do very well or very badly. The fact that the -0.3 cph peak also appears in the model calculations, suggests that the peak is not due to some characteristics of the individual floe, where the measurements were made. Inspection of the ice–current coherence in the model calculations showed that the significant area is too broad close to the surface and too narrow deeper down.

High-frequency fluctuations in the wind velocity could have been a reason to the high inertial energy. This was examined further by smoothing the wind data by removing frequencies higher than one cycle per day and running the full model with the smoothed wind. The simulations showed a slight damping in the ice and current velocities, and thus the high frequency regime in the wind adds a bit to the inertial energy in the model.

4.3. *Ocean model, prescribed ice drift*

The results from a simulation of the ocean model forced by measured ice velocities are shown in Fig. 8. As expected, the overall agreement between calculated and measured currents is much better. The largest discrepancy occurs again on days 11–12 at 20 m depth. It is also the period when the ice was forced with rather strong northerly winds. The currents at 20 m depth are almost in the opposite direction and could be interpreted as adjustment drift.

The currents seem to be quite well simulated. Thus we may conclude that the ice strongly resisted inertial oscillations, and also caused the damping of inertial oscillations in the currents. The damping can also be easily understood on the basis of a simple analytic model. Forcing the vertically integrated ocean equation with a constant ice motion and using a linear friction law gives exponential damping to the inertial oscillations with a relaxation time of about one day.

4.4. *Wind factor ice model*

The classical purely wind-driven free drift model of ice gives quite good results, see Fig. 9a. The parameters of the present free drift model are: wind factor equal to 1.9% and deviation angle equal to 21°. The good fit could, of course, already be foreseen from the high ice–wind correlation. Remarkably, the full ice–ocean model discussed in Subsection 4.2 does not give any better fit with the measurements than this simple wind factor model. The calculated–measured correlation for the wind factor ice model and the full ice–ocean model became 0.90 and 0.87, respectively.

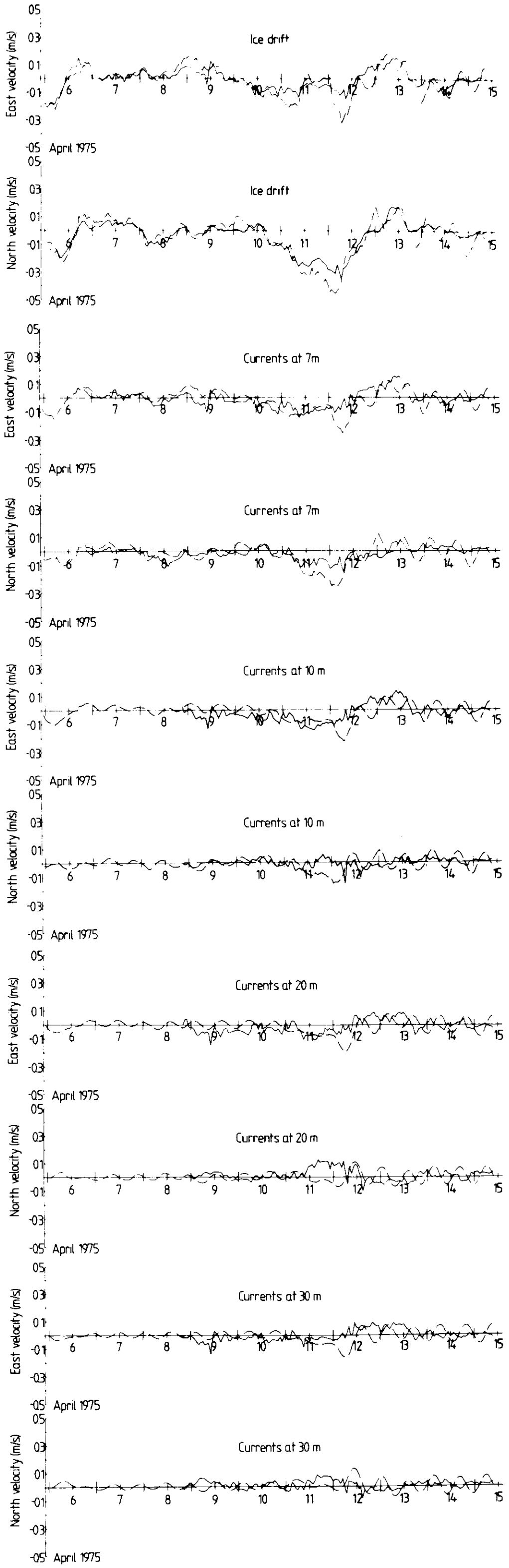

Fig. 7. Measured (solid lines) and calculated (broken lines) ice velocity and currents at 7, 10, 20 and 30 m below the ice–water interface. The calculations are according to the ice–ocean model.

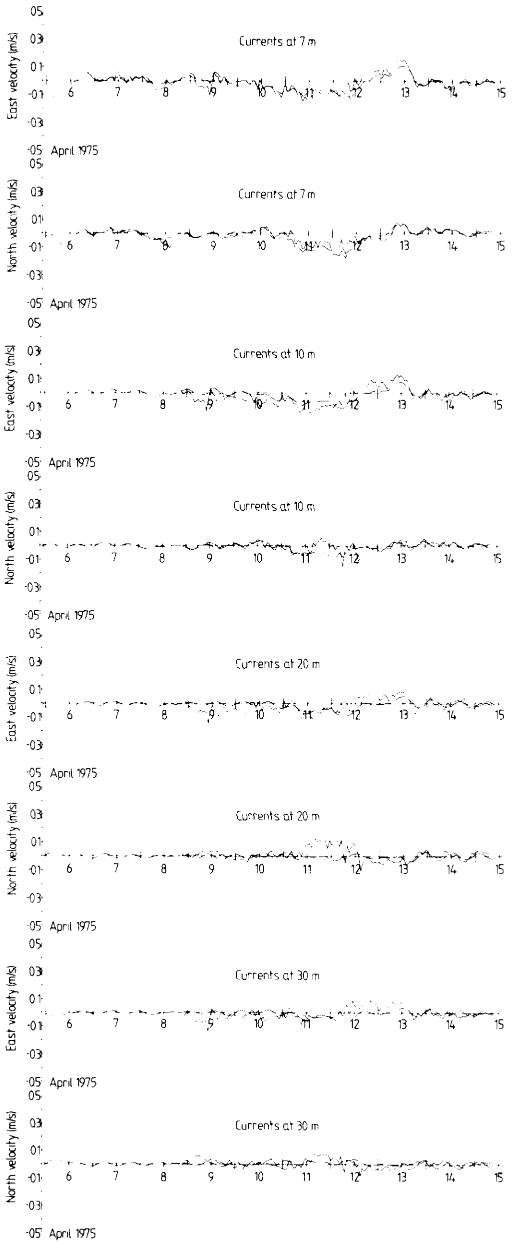

Fig. 8. Measured (solid lines) and calculated (broken lines) currents at 7, 10, 20 and 30 m below the ice–water interface. The calculations are according to the ocean model with prescribed ice drift.

A comparison between the two models shows that the main differences are due to the inertial oscillations, see Figure 9b.

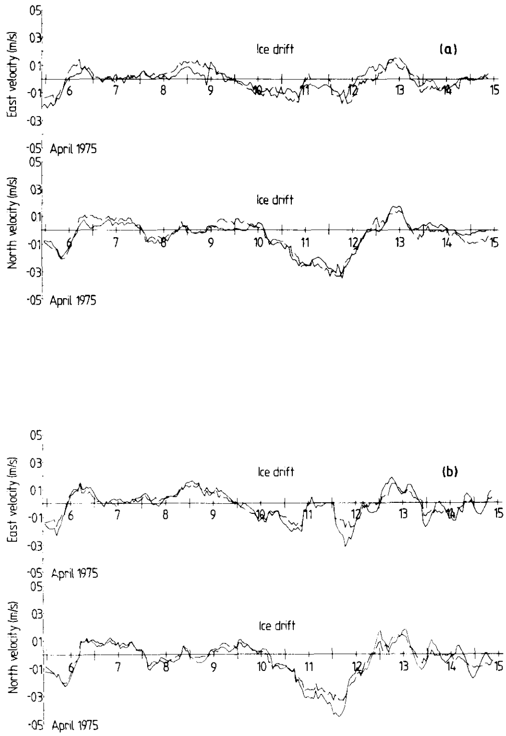

Fig. 9. Comparison between (a) measured ice drift (solid lines) and calculated ice drift based on the wind factor ice model (broken lines), and (b) the full ice–ocean model (solid lines) and the wind factor ice model (broken lines).

5. Other models

Further aspects of wind-forced ice motion can be learned from the ice–ocean model (e.g., effects of depth, stratification, and ice thickness and roughness variations). Comparisons with other seas and models may also give a deeper insight into the ice–ocean interaction.

5.1. *Free drift*

In Fig. 10, free ice drift in the Bering Sea is examined by comparing the present model with that of Overland et al. (1984). The present model, the time-dependent model, illustrates that the free drifting ice rapidly responds to the wind, with inertial oscillations around the mean drift. The steady state values by Overland et al. (1984) are slightly higher. The reason is that the present

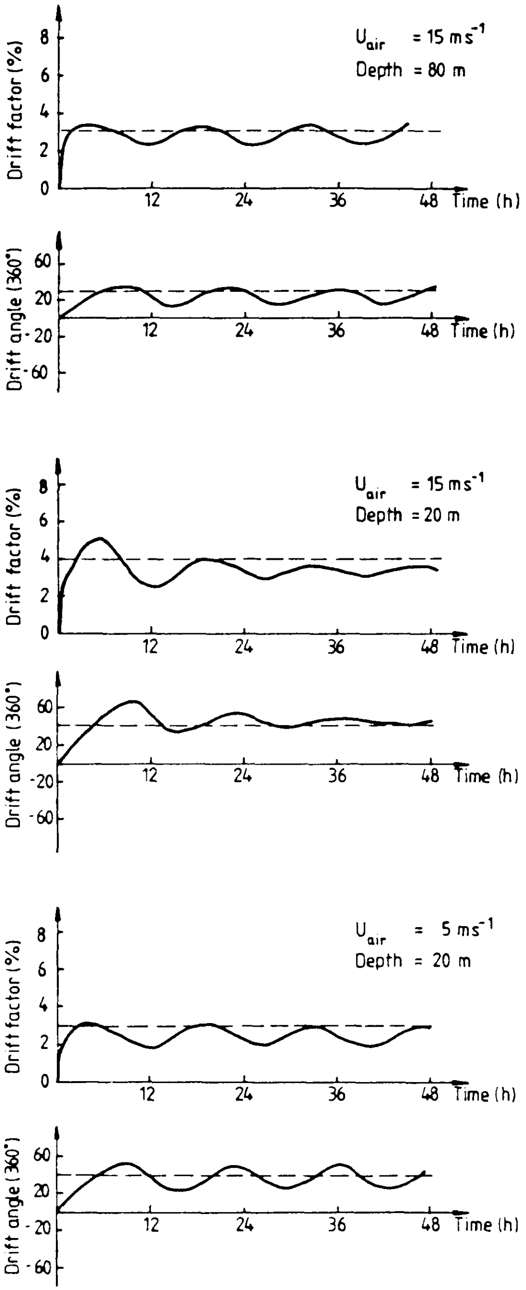

Fig. 10. A comparison between the present model (fully drawn lines) and that by Overland et al. (1984) (broken lines).

model predicts higher turbulent mixing and therefore a larger water stress, compared with the model used by Overland et al. (1984).

5.2. *Oceanic boundary layer*

The turbulence structure within the ocean boundary layer under drifting sea ice is illustrated in Fig. 11. In the figure, data from the Arctic Ocean, presented by McPhee and Smith (1976), are compared with the present model. In the calculation, both a neutral and a slightly stable surface layer are considered. The stratification is modelled with the salinity equation, and the values are taken from McPhee and Smith (1976). The agreement is reasonable, indicating that the upper 35 m are influenced by stratification. The measurements by McPhee and Smith (1976) have also been examined by Svensson (1981).

5.3. *Coupled models*

In ice–ocean thermodynamic studies, the main unknown heat flux is the heat from the ocean to the ice. This implies a need for coupled ice–ocean models, e.g., Lemke (1987) or Ikeda (1986). This is particularly true in the case of the marginal ice zone and during freezing and melting.

The interaction between turbulence and freezing or melting is not dealt with in the present

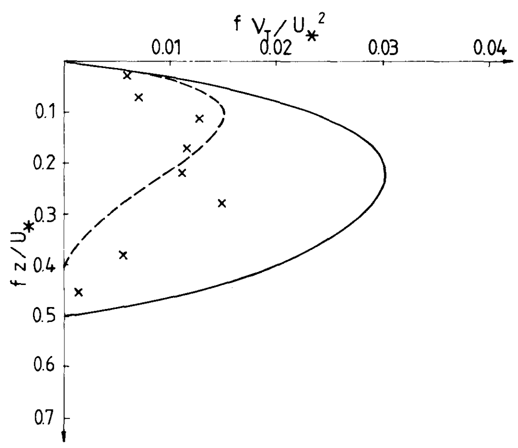

Fig. 11. Measured and calculated eddy-viscosity distribution. Crosses represent measurements from McPhee and Smith (1976). The fully drawn line represents calculated values without stratification and the dashed line calculates values with stratification in the upper 35 m. The friction velocity is denoted by u_*.

paper. Instead, the reader is referred to Mellor et al. (1986) or Svensson and Omstedt (1989).

In the latter paper, a mathematical model of the ocean boundary layer under melting ice is presented. The model is based on the conservation equations for heat, salt, and momentum in their one-dimensional forms and includes a low-Reynolds number turbulent model for the viscous region. In the outer region, the same turbulence model as in the present study is applied. Also a discrete element approach for the parameterization of ice keels is introduced.

6. Conclusions

The objective of the present study was to examine the dynamic coupling of ice and water for an ice field with free boundaries. For this purpose, ice drift, wind and current measurements from the Bothnian Bay were examined, using a transient ice–ocean model. Even though the data seemed to fulfill the conditions for almost ideal free drift, inertial oscillations in the ice drift were missing. In the boundary layer beneath the drifting ice, the inertial oscillations were also damped. It is concluded that internal friction within the ice is the most probable explanation.

The analysis also shows that for the present case the simple wind factor ice model works as well as the full coupled transient ice–ocean model. The reason is that the wind factor ice model does not resolve the inertial oscillations, a feature which after all should be the characteristic sign of an ideal free drift period. To improve the coupled ice–ocean modelling significantly, internal ice friction and thus horizontal ice processes have to be resolved.

7. Acknowledgements

This work is a part of the Swedish/Finnish Winter Navigation Research Programme, funded by the Swedish Administration of Shipping and Navigation and the Finnish Board of Navigation. Special thanks are given to the reviewers for valuable comments.

REFERENCES

Egger, J. and Schmid, S. 1988. Elimination of spurious inertial oscillations in boundary layer models with time-dependent geostrophic winds. *Boundary-Layer Meteorology 43*, 393–402.

Gustafson, T. and Kullenberg, B. 1936. An investigation of inertial currents in the Baltic Sea. Svenska Hydrografisk-Biologiska Kommissionens skrifter, *serie: Hydrografi XIII*, 28 pp.

Ikeda, M. 1985. A coupled ice–ocean model of a wind-driven coastal flow. *J. Geophys. Res. 90, C5*, 9119–9128.

Ikeda, M. 1986. A mixed-layer beneath melting sea ice in the Marginal Ice Zone using a one-dimensional turbulent closure model. *J. Geophys. Res. 91, C4*, 5054–5060.

Joffre, S. M. 1984. The atmospheric boundary layer over the Bothnian Bay; a review of work on momentum transfer and wind structure. Winter Navigation Research Board, *Report No. 40*, Helsinki, Finland, 58 pp.

Kahma, K. K. and Leppäranta, M. 1981. On errors in wind speed observations on R/V Aranda. *Geophysica 17*, 155–165.

Lagerloef, G. S. and Muench, R. D. 1987. Near-inertial current oscillations in the vicinity of the Bering Sea Marginal ice zone. *J. Geophys. Res. 92, C11*, 11789–11802.

Lemke, P. 1987. A coupled one-dimensional sea ice–ocean model. *J. Geophys. Res. 92, C12*, 13164–13172.

Leppäranta, M. 1981. On the structure and mechanics of pack ice in the Bothnian Bay. *Finnish Marine Research 248*, 3–86.

Leppäranta, M. 1989. Observations of free ice drift and currents in the Bay of Bothnia. *Göteborgs Kungliga Vetenskaps—och Vitterhetssamhällets Acta, Ser. Geofys. 3*, in press.

Leppäranta, M. and Hibler III, W. D. 1985. The role of plastic ice interaction in marginal ice zone dynamics. *J. Geophys. Res. 90, C11*, 11899–11909.

Leppäranta, M. and Hibler III, W. D. 1987. Mesoscale sea ice deformation in the East Greenland marginal ice zone. *J. Geophys. Res. 92, C7*, 7060–7070.

McPhee, M. G. 1978. A simulation of inertial oscillation in drifting pack ice. *Dyn. of Atm. and Oceans 2*, 107–122.

McPhee, M. G. and Smith, J. D. 1976. Measurements of the turbulent boundary layer under pack ice. *J. of Physical Ocean. 6*, 696–711.

Martin, S. and Becker, P. 1987. High-frequency ice floe collisions in the Greenland Sea during the 1984 marginal ice zone experiment. *J. Geophys. Res. 92*, 7071–7084.

Mellor, G. L., McPhee, M. G. and Steele, M. 1986. Ice–sea water turbulent boundary layer interaction with melting or freezing. *J. Phys. Oceanogr. 16*, 1829–1846.

MIZEX Group, 1986. MIZEX East 83/84: The summer marginal ice zone program in the Fram Strait/Greenland Sea. *EOS, Transactions of the American Geophysical Union 67, 23*, 513–517.

Oke, T. R. 1981. *Boundary layer climates*. New York: Methuen & Co.

Omstedt A. 1980. A sensitivity analysis of steady, free floating ice. *SMHI Reports*, RMK 19, SMHI, S-601 76 Norrköping, Sweden.

Omstedt, A., Sahlberg, J. and Svensson, U. 1983. Measured and numerically simulated autumn cooling in the Bay of Bothnia. *Tellus 35A*, 231–240.

Ono, N. 1978. Inertial period motions of drifting sea ice. *Low Temperature Science, Ser. A*, 37 (in Japanese, with English summary), 107–113.

Overland, J. E., Mofjeld, H. O. and Pease, C. H. 1984. Wind-driven ice drift in a shallow sea. *J. Geophys. Res. 89*, 6525–6531.

Rodi, W. 1987. Examples of calculation methods for flow and mixing in stratified flows. *J. Geoph. Res. 92*, 5305–5328.

Røed, L. P. and O'Brien, J. J. 1983. A coupled ice–ocean model of upwelling in the marginal ice zone. *J. Geophys. Res. 88*, 2863–2872.

Svensson, U. 1979. The structure of the turbulent Ekman layer. *Tellus 31*, 340–350.

Svensson, U. 1981. On the influence of buoyancy on the turbulent Ekman layer. *Proc. of the Third Symposium on Turbulent Shear Flows*. New York: Springer Verlag, 12.5–12.11.

Svensson, U. 1986. *The PROBE Manual*. SMHI, Rapport Oceanografi No. 10, S-601 76 Norrköping, Sweden.

Svensson, U. and Omstedt, A. 1989. A mathematical model of the ocean boundary layer under drifting melting ice. *J. Phys. Oceanogr.*, in press.

Wadhams, P., Martin, S., Johannessen, O. M., Hibler III, W. D. and Campbell, W. J. 1981. MIZEX. A program for mesoscale air–ice–ocean interaction experiments in Arctic marginal ice zones (I). *Research strategy. CRREL Special Report 81–19*, U.S. Army Cold Regions Research and Engineering Laboratory, Hanover, N.H., USA. 20 pp.